

Calibration of Multi-Axis MEMS Force Sensors Using the Shape from Motion Method

Yu Sun, Keekyoung Kim

*Advanced Micro and Nanosystems Lab
University of Toronto
Canada*

sun, kkim@mie.utoronto.ca

Richard M. Voyles

*Collaborative Systems Lab
University of Minnesota
U.S.A.*

voyles@cs.umn.edu

Bradley J. Nelson

*Inst. of Robotics and Intelligent Systems
Swiss Federal Inst. of Technology - Zürich
Switzerland*

bnelson@ethz.ch

Abstract - This paper presents a new design of a two-axis MEMS (microelectromechanical systems) capacitive force sensor with strict linearity and a new sensor calibration method for micro-sensors. Precise calibration of multi-axis micro force sensors is difficult for several reasons, including the need to apply many known force vectors at precise orientations at the micro force scale, and the risk of damaging the small, fragile MEMS device. In this paper the shape from motion method is introduced for micro force sensors resulting in a rapid and effective calibration technique. Structural-electrostatic coupled field simulations are conducted in order to optimize the sensor design, which is calibrated with the shape from motion method as well as the least squares method for comparison purposes. Calibration results demonstrate that the shape from motion method is an effective, practical, and accurate method for calibrating multi-axis micro force sensors.

Index Terms - MEMS force sensor, multi-axis, calibration, shape from motion

I. INTRODUCTION

The accurate measurement of small forces is crucial for realizing force-controlled micromanipulation and for understanding many fundamental processes of biological systems. There are five basic mechanisms used to measure forces: (a) balancing the unknown force against a standard mass through a system of levers; (b) measuring the acceleration of a known mass; (c) equalizing the force to a magnetic force or an optical force generated by the interaction of a current-carrying coil and a magnet or by the interaction of a laser beam and a trapped bead; (d) distributing the force over a specific area to generate pressure and then measuring the pressure, based on which the force is indirectly derived; and (e) converting the applied force into the deformation of an elastic element.

In the case of MEMS capacitive force sensors [1][2][3], small deflections caused by applied forces are transduced into detectable capacitance changes. An electronic circuit converts the capacitance variations into DC-voltage variations. With their ability to measure forces from the mN (10^{-3} Newton) to nN (10^{-9} Newton) range, MEMS capacitive force sensors are suitable for a wide range of biological studies that provide not only qualitative but also quantitative information on the cellular, sub-cellular, and organism levels. These measurements are instrumental in understanding the

fundamental elements of biological systems. Due to their high performance and their ability to measure forces along multiple axes, capacitive MEMS force sensors are powerful alternatives to other MEMS transducers, such as cantilever-based sensors [4][5][6]. Compared to force measurement techniques such as optical tweezers [7][8], ultra fine glass needles (also known as the microneedle technique) [9][10], atomic force microscopy (AFM) [11][12][13][14], the magnetic bead measurement method [15][16][17], and micropipette aspiration [18][19], MEMS capacitive force sensors provide the following advantages: (a) they are capable of measuring a wide range of forces from mN to pN (10^{-12} Newton); (b) they are capable of providing force information along multiple axes; (c) they provide the most direct means of force measurement instead of indirectly obtaining force information from pressure measurements; (d) they have the advantage of low power, low noise, high sensitivity, and insensitivity to temperature variation; and (e) batch microfabrication processes are capable of manufacturing hundreds of these transducers simultaneously, making them cost effective.

Although multi-axis capacitive micro force sensors can be produced by microfabrication with a high yield, calibrating these small, fragile multi-axis devices is time consuming and risky in terms of device destruction. This paper presents a shape from motion calibration technique and its application to calibrating multi-axis micro force sensors. The method is based on an extension of a computer vision technique for determining an object's 3D shape based on a sequence of 2D images [20]. Although multi-axis capacitive micro force sensors are used as an example, the shape from motion calibration method is not limited to the capacitive sensing mechanism or to force transduction [21].

Common methods of sensor calibration employ a tedious scheme that requires many readings from the sensor under precisely known loading conditions. A least squares method is typically used to combine these readings into a best-fit calibration matrix. In contrast, the shape from motion method uses a large number of unknown forces applied to the multi-axis force sensor in random directions. These forces are related through the simple constraint that all applied calibration forces are of the same magnitude. Using singular value decomposition, both the calibration matrix and the applied forces are extracted from this large number of "arbitrary" measurements and one single precise force input.

Thus, accurate calibration can be achieved with much less effort than the traditional scheme, since the majority of the measurements do not require precisely known force inputs, the uncertainty of which introduces an additional error source.

For capacitive multi-axis micro force sensors, the shape from motion calibration method eliminates the use of comb drive actuation for “self-testing”, which requires a dedicated chip area for actuation comb drives. The “self-testing” technique is also limited by the intrinsic pull-in limit [22] which makes full-range calibration infeasible. Furthermore, the shape from motion calibration method minimizes the possibility of damaging the tiny, fragile micro force sensors during calibration.

This paper presents a new design of a two-axis capacitive micro force sensor with strict linearity. A coupled structural-electrostatic finite element simulation is conducted. The sensor is calibrated with the shape from motion method as well as the least squares method for comparison purposes. Calibration results demonstrate that the shape from motion method is an effective, practical, and accurate method for calibrating multi-axis micro force sensors.

II. MULTI-AXIS FORCE SENSOR CALIBRATION

A multi-axis force sensor converts an applied force vector, \mathbf{m} , into a measurement vector, \mathbf{z} . If the system is *linear*, the calibration function, which is a constant matrix \mathbf{C} , transforms \mathbf{z} into \mathbf{m} as

$$\mathbf{C}\mathbf{z} = \mathbf{m} \text{ or } \mathbf{z}^T \mathbf{C}^T = \mathbf{m}^T \quad (1)$$

With the calibration matrix known, applied forces are resolved from given measurement vectors.

A. Least Squares Calibration

The most common technique for force sensor calibration is the least squares method, which requires that many exactly known force vectors, \mathbf{m}_i , are applied to the multi-axis force sensor and the corresponding sensor output (i.e., the measurement vectors, \mathbf{z}_i) measured. Then, (1) becomes

$$\begin{bmatrix} \mathbf{z}_1^T \\ \vdots \\ \mathbf{z}_n^T \end{bmatrix} \mathbf{C}^T = \begin{bmatrix} \mathbf{m}_1^T \\ \vdots \\ \mathbf{m}_n^T \end{bmatrix} \text{ or } \mathbf{Z}^T \mathbf{C}^T = \mathbf{M}^T \quad (2)$$

The calibration matrix, \mathbf{C}^T can be obtained by the pseudo-inverse of the measurement matrix, \mathbf{Z}

$$\mathbf{C}^T = \mathbf{Z}^+ \mathbf{M} \quad (3)$$

The precise application of force vectors makes the least squares calibration process tedious for macro-scaled force sensors and extremely difficult to implement for micro-scaled force sensors. The error in applied force vectors must be minimized for an accurate calibration, because the error manifests itself directly in the calibration matrix. This error can only be minimized by exercising extreme care when applying forces during calibration. Thus, incorporating a large number of redundant data points in the least squares calibration is difficult and time consuming due to the error minimization requirement of applied forces.

B. Shape from Motion Calibration

Unlike the least squares calibration method, the shape from motion method [21] does not require the application of exactly known forces, but only a constraint that relates them (i.e., force magnitude must be *constant*). Therefore, redundant force vectors and corresponding measurement vectors can be obtained rapidly to establish the calibration matrix. A small number of exactly known applied forces are used to establish the reference data frame, but none of the redundant data requires precisely applied forces. The ability to readily and rapidly collect and apply massive amounts of redundant data in shape from motion calibration accounts for its significant advantage over the conventional least squares method.

In the shape from motion calibration approach, the calibration matrix encodes the mechanical structure of the force sensor, including the placement of sensing elements and the properties of the material from which it is made. These are what define the sensor’s intrinsic shape. The motion refers to the movement of the applied forces around the sensor. Shape from motion refers to the fact that the shape of the force sensor can be recovered by knowing the theoretical rank of the shape and applying arbitrary motion to the force.

The derivation of the shape from motion calibration algorithm begins with the following representation of the sensor function

$$\mathbf{z}_i^T = \mathbf{m}_i^T \mathbf{S} \quad (4)$$

where \mathbf{z}_i^T is a $1 \times p$ measurement vector, \mathbf{m}_i^T is a $1 \times m$ load vector, and \mathbf{S} is the $m \times p$ shape matrix. There are p sensing elements and m degrees-of-freedom. From (1), the calibration matrix, \mathbf{C} can be derived from the shape matrix \mathbf{S}

$$\mathbf{C} = \left[\mathbf{S}^T \right]^+ \quad (5)$$

If n force vectors are applied and corresponding measurements are collected, (4) can be re-written as

$$\mathbf{Z} = \mathbf{M} \mathbf{S} \quad (6)$$

where \mathbf{Z} is the $n \times p$ measurement matrix and \mathbf{M} is the $n \times m$ matrix that represents the motion matrix encoding the forces applied to the sensor.

From a singular value decomposition, \mathbf{M} and \mathbf{S} can be determined simultaneously with a given \mathbf{Z} . SVD produces a unique decomposition from any $n \times p$ matrix

$$\mathbf{Z} = \mathbf{U} \mathbf{\Sigma} \mathbf{V}^T \quad (7)$$

where \mathbf{U} is an $n \times n$ orthogonal matrix, $\mathbf{\Sigma}$ is a $n \times p$ diagonal matrix of the singular values of \mathbf{Z} in descending order, and \mathbf{V} is a $p \times p$ orthogonal matrix.

Assuming the proper rank of \mathbf{Z} is r , the best projection of \mathbf{Z} onto an r -dimensional space (for $r \leq p$) is

$$\mathbf{Z}^* = \mathbf{U}^* \mathbf{\Sigma}^* \mathbf{V}^{*T} \quad (8)$$

where \mathbf{U}^* consists of the first r columns of \mathbf{U} , $\mathbf{\Sigma}^*$ is a diagonal matrix of the first r singular values, and \mathbf{V}^{*T} consists of the first r rows of \mathbf{V}^T . Combining (6) and (8) yields,

$$\mathbf{U}^* \mathbf{\Sigma}^* \mathbf{V}^{*T} = \hat{\mathbf{M}} \hat{\mathbf{S}}$$

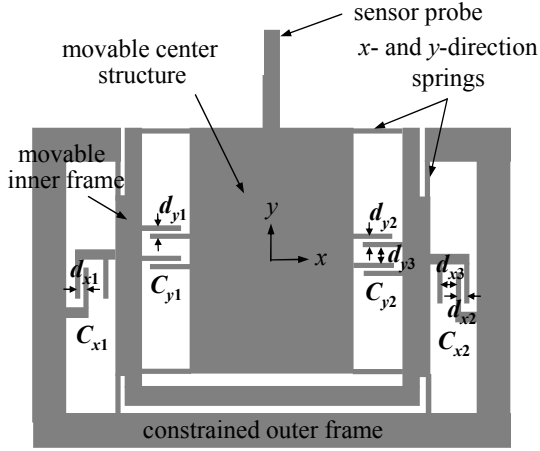


Fig. 1 Design of a two-axis micro force sensor with two decoupled frames and differential tri-plate comb drives along both x and y directions.

$$\hat{\mathbf{M}} = \mathbf{U}^* (\hat{\Sigma}^*)^{1/2} \quad (9)$$

$$\hat{\mathbf{S}} = (\hat{\Sigma}^*)^{1/2} \mathbf{V}^{*\text{T}}$$

At this stage, $\hat{\mathbf{M}}$ and $\hat{\mathbf{S}}$ are not yet the true motion and shape matrices. Introducing an affine transformation, given any invertible $r \times r$ matrix \mathbf{A} , produces an equivalent decomposition

$$\hat{\mathbf{M}}\hat{\mathbf{S}} = (\hat{\mathbf{M}}\mathbf{A}^{-1})(\mathbf{A}\hat{\mathbf{S}}) \quad (10)$$

Then, the motion and shape matrices can be written as

$$\mathbf{M} = \hat{\mathbf{M}}\mathbf{A}^{-1} \text{ and } \mathbf{S} = \mathbf{A}\hat{\mathbf{S}} \quad (11)$$

where \mathbf{A}^{-1} is a particular affine transformation that enforces the previously mentioned constraint relating the measurements. In order to solve \mathbf{A}^{-1} , a geometric constraint can be applied to the individual vectors of the motion matrix. Once \mathbf{A} is known, \mathbf{S} and \mathbf{C} can be obtained from (11) and (5). Finally, precise measurements are introduced to orient the calibration matrix with respect to the desired reference frame and to scale the results to the desired engineering units.

III. MODELING AND SIMULATION

A. Design of a Two-Axis Capacitive Micro Force Sensor

Fig. 1 shows a schematic drawing of the two-axis micro force sensor design. The sensor probe transmits forces deflecting the unidirectionally compliant springs in the x and y directions. The deflection displaces the movable center structure and the movable capacitor plates (i.e., comb fingers). Total capacitance changes resolve applied forces. The two decoupled frames (i.e., the movable inner frame and the outer constrained frame) avoid the rotation of the movable center structure and capacitor plates, thus, promising strict linearity, which is an improvement over the previous two-axis designs [1]. The decoupled-frame design guarantees that forces are directly transmitted from the sensor probe to the centroid of the movable center structure. When the x component of an applied force is along the positive x -direction, the gap d_{x1} in C_{x1} increases while the gap d_{x2} in C_{x2} decreases. Capacitance varies according to

$$C_{x1} = n \frac{\epsilon_0 t l}{d_{x1} - x} + n \frac{\epsilon_0 t l}{d_{x2} + x} \quad (12)$$

$$C_{x2} = n \frac{\epsilon_0 t l}{d_{x1} + x} + n \frac{\epsilon_0 t l}{d_{x2} - x} \quad (13)$$

where n is the number of comb finger pairs, t and l are comb finger thickness and length, and x is the displacement caused by the x -component of applied forces. Such comb drive configurations are based on a previous differential tri-plate comb drive design [3]. Using a differential capacitive voltage divider circuit [3], sensor output from forces applied in the x direction, V_{out-x} is

$$V_{out-x} = V_s \left(\frac{C_{x1} - C_{x2}}{C_{x1} + C_{x2}} \right) \quad (14)$$

Similar to (12)-(14), a symmetrical description applies to the y direction.

Sensor stiffness is determined by the spring dimensions. The springs are modeled as beams with two fixed ends in both x and y with a point load applied in the middle. The force-deflection model is

$$\Delta d = \frac{Fl^3}{4Ew^3t} \quad (15)$$

where F is the x - or y -component of an applied force, E is the Young's modulus of silicon, and l , w , and t are spring length, width, and thickness. Fig. 2 shows a solid model of the two-axis micro force sensor design, and Table 1 summarizes the design specifications.

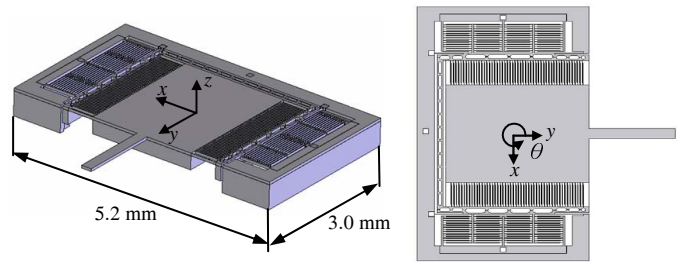


Fig. 2 (a) Solid model of the two-axis capacitive micro force sensor design with the x - y - z coordinate frame defined. (b) For calibration, the sensor is mounted vertically, for example to a stepper motor, so that the weight of the movable parts of the sensor acts as a constant-magnitude load to the sensor as the complete sensor frame is rotated counter-clockwise around the z -axis. The schematic shows the initial sensor orientation at zero degree.

TABLE I
SENSOR DESIGN SPECIFICATIONS.

Base	5.2 mm \times 3.0 mm \times 0.5 mm
Sensor probe	0.2 mm \times 1.5 mm \times 50 μ m
Movable center	2 mm \times 2.5 mm \times 0.3 mm
Capacitance plates	0.45 mm \times 5 μ m \times 50 μ m
Springs	0.5 mm \times 4 μ m \times 50 μ m
Spring Stiffness	16.384 N/m
Overlap area ($t \times l$)	50 μ m \times 400 μ m
Gap between combs ($d_{x1,2}$ and $d_{y1,2}$)	5 μ m
Gap between combs (d_{x3} and d_{y3})	30 μ m
Number of comb finger pairs (n)	52

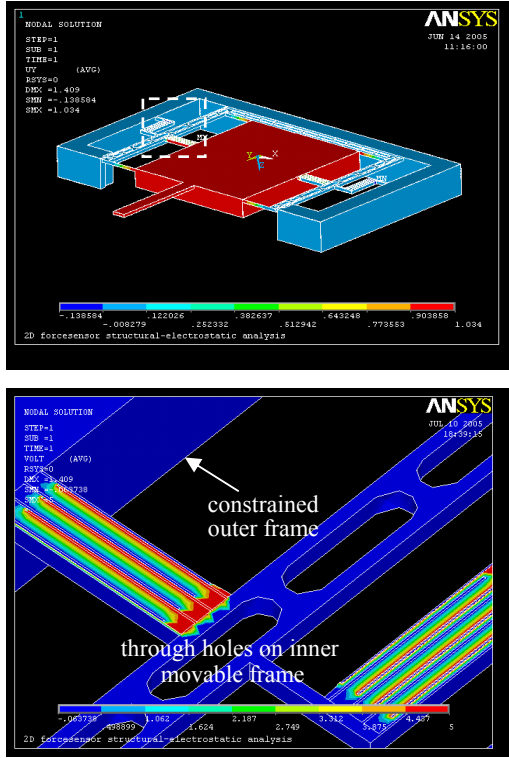


Fig. 3 Structural-electrostatic coupled simulation. (a) Finite element model. (b) Zoom-in view of the boxed area in (a). The color changes represent electric potential distribution that changes with applied forces.

B. Structural-Electrostatic Coupled Simulation

The two-axis micro force sensors can be microfabricated using a deep-reactive-ion-etching (DRIE) on silicon-on-insulator (SOI) recipe [3]. In order to calibrate the sensor using the shape from motion method, the sensor is mounted vertically, for example to a stepper motor, so that the weight of the movable parts of the sensor acts as a constant-magnitude load to the sensor as the complete sensor frame is rotated counter-clockwise around the z -axis (Fig. 2(b)). When the sensor is rotated, the gravity force of the movable parts of the sensor loads the suspended x and y springs. The movable parts include the sensor probe, center structure, suspended springs, movable comb fingers, and the inner frame. Through-holes are constructed on the movable inner frame to minimize the mismatch of the gravity force on the x and y directional springs during rotation (Fig. 3(b)). In this design, the gravity force of the inner frame and the sensor probe are made negligible compared to the movable center structure. Although the gravity force always applies to the centroid of the movable center structure during rotation, it is equivalent to a direct application of forces of an equal magnitude to the sensor probe. Thus, no transformation is needed from the centroid of the movable center structure to the sensor probe. Structural-electrostatic coupled finite element simulation is conducted using ANSYS®, in which electrical potential energy E in the comb drive sets is obtained from gap changes between comb finger pairs caused by applied forces. Capacitance is subsequently obtained from the electrical potential energy.

$$C = \frac{2E}{V^2} \quad (16)$$

IV. RESULTS AND DISCUSSION

A. Shape from Motion Calibration

Initially, let us assume a noise-free calibration procedure. The gravity force of the movable parts serves as a constant-magnitude force applying in random directions in the x - y plane to the force sensor with x - y plane defined in Fig. 2(b). In simulation, the force sensor is rotated in two-degree steps for a total of 360 degrees. In practice, the 181 measurement points can be readily obtained by rotating the sensor around the z axis with a stepper motor. From (4),

$$[z_{i1} \ z_{i2}] = [\cos \theta_i \ \sin \theta_i] \begin{bmatrix} s_{11} & s_{12} \\ s_{21} & s_{22} \end{bmatrix}$$

or

$$[V_{ix} \ V_{iy}] = [F_{ix} \ F_{iy}] \begin{bmatrix} s_{11} & s_{12} \\ s_{21} & s_{22} \end{bmatrix} \quad (17)$$

The force has been arbitrarily set to one unit, leaving only $\cos \theta$ and $\sin \theta$ in the motion matrix, \mathbf{M} . This gives a motion constraint equation as

$$\mathbf{M} \mathbf{M}^T = 1 \text{ or } \cos^2 \theta + \sin^2 \theta = 1 \quad (18)$$

The rank of the shape matrix is at most 2 so that the proper rank of the $n \times p$ measurement matrix, \mathbf{Z} , is also 2. Denote the elements of \mathbf{A}^{-1} by a_{11} , a_{12} , a_{21} , and a_{22} and the i th row of $\hat{\mathbf{M}}$ by m_{i1} and m_{i2} , then substitute (11) into (18)

$$m_{i1}^2 (a_{11}^2 + a_{12}^2) + 2m_{i1}m_{i2} (a_{11}a_{21} + a_{12}a_{22}) + m_{i2}^2 (a_{21}^2 + a_{22}^2) = 1 \quad (19)$$

where the coefficients of the quadratic equation ($a_{11}^2 + a_{12}^2$), ($a_{11}a_{21} + a_{12}a_{22}$), and ($a_{21}^2 + a_{22}^2$) can be solved with the least squares method. Then, the individual a_{ij} values can be obtained numerically with the assumption of $a_{12} = a_{21}$ or $a_{21} = 0$. The symmetrical upper triangular matrix, \mathbf{A} , ensures invertibility. With \mathbf{A}^{-1} , the shape matrix \mathbf{S} is solved using (11) and the calibration matrix \mathbf{C} is solved using (5). At this stage, however, the resulting calibration matrix \mathbf{C} is not yet oriented in any particular direction. To align it with the desired reference frame, only one precise load (i.e., a \mathbf{z} , \mathbf{m} pair, both vectors known) is needed to rotate and scale the calibration matrix appropriately.

$$\mathbf{C}_o = \text{Rot}(\phi) \frac{\|\mathbf{m}\|}{\|\mathbf{Cz}^T\|} \mathbf{C} = \begin{bmatrix} 0.2848 & -0.0001 \\ 0.0002 & -0.2877 \end{bmatrix} \quad (20)$$

where \mathbf{C}_o is the final, oriented calibration matrix, ϕ is the angular difference between \mathbf{m} and \mathbf{Cz} , and $\text{Rot}(\phi)$ is the 2×2 rotation matrix. Fig. 4 shows a plot of the recovered motion (i.e., forces) from one calibration trial. The motion demonstrates nearly perfect average circularity that verifies the validity of the calibration results. The cross in the plot corresponds to the calibration data point when the sensor is oriented along the 180-degree direction.

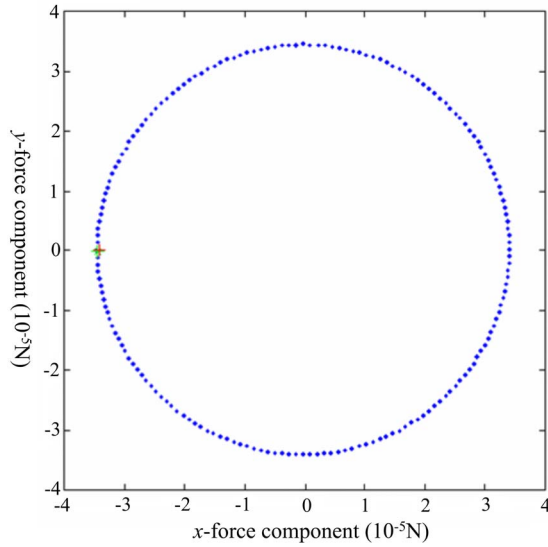


Fig. 4 Plot of the recovered motion (i.e., forces) from one calibration trial.

B. Comparison to Least Squares Method

In order to compare the shape from motion method to the conventional least squares method, 20 known data pairs (i.e., measurement vectors and precise force vectors) from simulation are used to obtain the least squares calibration matrix from (2)

$$\mathbf{C}_{LS-20} = \begin{bmatrix} 0.2845 & -0.0003 \\ 0.0000 & -0.2900 \end{bmatrix} \quad (21)$$

Another 181 known data pairs are used to verify the accuracy of the sensor output based on the shape from motion calibration matrix and the least squares matrix. Fig. 5 shows the sensor force estimates based on the corresponding sensor voltage output along the x and y directions and the calibration matrices obtained from the shape from motion method and the least squares method. We argue, for multi-axis sensors, the orthogonality of the force components is the most important metric of performance. To compare this, we look at the circularity of the resulting constant magnitude vectors (as in the plot in Fig. 4). A metric of the circularity is the standard deviation of the magnitude of these vectors. If the standard deviation is zero, the plot is a perfect circle. For the shape from motion method, the circularity metric is 0.0802, while it is 0.1390 for the least squares method. Furthermore, the average accuracy of the x and y components of the estimated force vectors for the shape from motion method is 0.502% in the x direction and 0.495% in the y direction. The corresponding error numbers for the least squares method are 0.586% in the x direction and 0.707% in the y direction.

When the same number of data points is used for the least squares method (181 precisely applied loads, which is unrealistic in practice), an improved calibration matrix results,

$$\mathbf{C}_{LS-181} = \begin{bmatrix} 0.2848 & -0.0000 \\ 0.0000 & -0.2877 \end{bmatrix} \quad (22)$$

the circularity of the least squares result is 0.0787, which is

comparable and slightly more accurate than the result for the shape from motion method. The average accuracy of the x and y components from the least squares method is also slightly better than the shape from motion method, 0.498% in the x direction and 0.456% in the y direction but, again, they are comparable. In reality, errors in the applied loads used in the least squares method tend to sacrifice orthogonality for average performance.

Thus, the benefit of the shape from motion method is a higher accuracy (comparing the results of 181 shape from motion data points to 20 least squares data points) with less effort and much less chance of damage to the small, fragile MEMS force sensors. Even when comparing an equivalent number of data points for each method, which is unrealistic for the least squares method due to the level of effort involved, the two techniques produce comparable performance.

The measurement vectors and force vectors used for the above comparisons do not include noise. In order to investigate how noise affects calibration results, uniformly distributed random noise on the interval of $[-1\text{mV}, 1\text{mV}]$ is injected into the measurement vectors and $[-0.1\mu\text{N}, 0.1\mu\text{N}]$ into the force vectors. For the shape from motion method, the

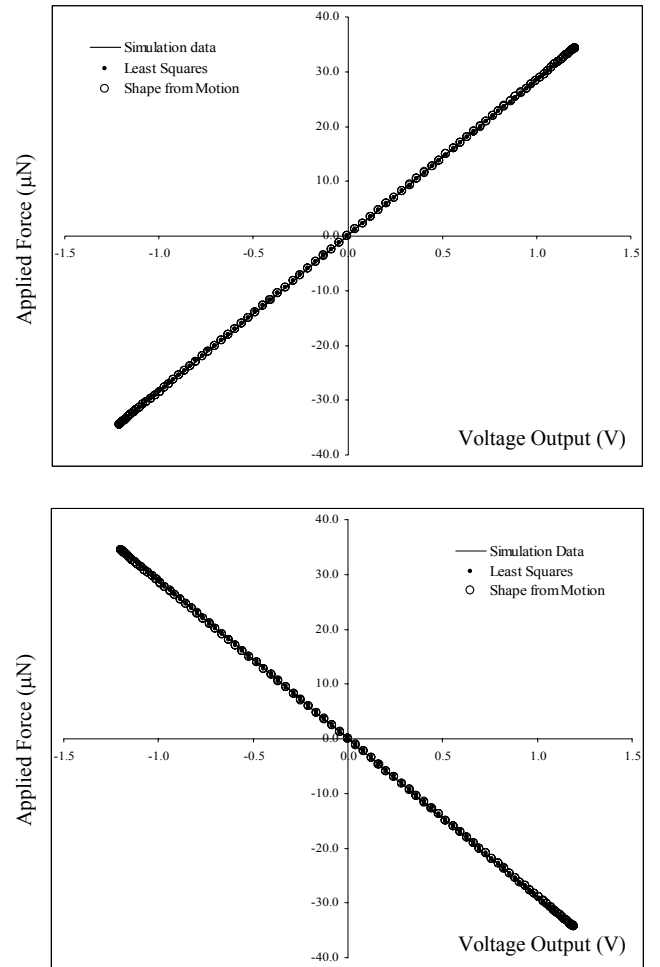


Fig. 5 Force estimates based on the least square calibration method and the shape from motion calibration method in the x and y directions.

circularity metric deteriorates from 0.0802 to 0.0814, and the average accuracy of the x and y components of the estimated force vectors becomes 0.508% in the x direction and also 0.508% in the y direction, which demonstrates that the shape from motion method has a strong noise rejection capability. With random noise injected, the least squares method based on 20 known data pairs produces a circularity metric of 0.1406 compared to 0.1390 in the noise-free case, and the average accuracy of the x and y components of the estimated force vectors becomes 0.595% in the x direction and 0.741% in the y direction.

It must be noted that the shape from motion method is not equivalent to gravity-based calibration. Although loads from the weight of the movable center structure can be estimated and treated as known forces at each sensor orientation, they are assumed to be unknown in the shape from motion calibration method. Thus, possible load errors from the estimate of the weight of the movable center structure and practical sensor orientation control are avoided. In the calibration of the two-axis capacitive micro force sensor, only one known load vector is used and all the other redundant data are collected from the rotation process.

V. CONCLUSION

This paper presents the design of a two-axis MEMS capacitive force sensor with strict linearity. The shape from motion method is introduced into the domain of calibrating multi-axis micro force sensors. Practically, the shape from motion calibration approach allows for collecting many more data points with less time, less effort, greater accuracy, and lower possibilities of damaging the small, fragile MEMS force sensors compared to the least squares method. Additionally, the shape from motion calibration method demonstrates a strong capability of noise rejection. In order to apply the shape from motion calibration method, two necessary conditions must be satisfied: (i) the multi-axis micro force sensor is a linear system; (ii) the applied force magnitude is constant. Although in this paper the shape from motion method is used to calibrate the two-axis capacitive micro force sensors, it is not limited to the capacitive sensing mechanism and can be extended to three-axis and six-axis sensor calibration [21].

ACKNOWLEDGMENTS

This research was supported by the Natural Sciences and Engineering Research Council of Canada through a Discovery Grant (#458099) and a Strategic Grant (#457292).

REFERENCES

- [1] Y. Sun, B.J. Nelson, D.P. Potasek, and E. Enikov, "A bulk microfabricated multi-axis capacitive cellular force sensor using transverse comb drives," *Journal of Micromechanics and Microengineering*, Vol. 12, pp. 832-840, 2002.
- [2] Y. Sun, K.T. Wan, B.J. Nelson, J. Bischof, and K. Roberts, "Mechanical property characterization of the mouse zona pellucida," *IEEE Trans. on NanoBioScience*, Vol. 2, pp. 279-286, 2003.
- [3] Y. Sun, S.N. Fry, D.P. Potasek, D.J. Bell, and B.J. Nelson, "Characterizing fruit fly flight behaviour using a microforce sensor with a new comb drive configuration," *J. of Microelectromechanical Systems*, Vol. 14, pp. 4-11, 2005.
- [4] G. Lin, K.S. Pister, and K.P. Roos, "Surface micromachined polysilicon heart cell force transducer," *J. of Microelectromechanical Systems*, Vol. 9, pp. 9-17, 2000.
- [5] G.G. Guilbault and J.H. Luong, "Biosensors: current status and future possibilities," *Selective Electrode Review*, Vol. 11, pp. 3-16, 1989.
- [6] M.E. Fauver, D.L. Dunaway, D.H. Lillienfeld, H.G. Craighead, and G.H. Pollack, "Microfabricated cantilevers for measurement of subcellular and molecular forces," *IEEE Trans. on Biomedical Engineering*, Vol. 45, pp. 891-898, 1998.
- [7] W.H. Wright, G.J. Sonek, Y. Tadir, and M.W. Berns, "Laser trapping in cell biology," *IEEE J. of Quantum Electronics*, Vol. 26, pp. 2148-2157, 1990.
- [8] J. Conia, B.S. Edwards, and S. Voelkel, "The micro-robotic laboratory: optical trapping and scissoring for the biologist," *J. of Clinical Laboratory Analysis*, Vol. 11, pp. 28-38, 1997.
- [9] A. Kishino and T. Yanagada, "Force measurements by micromanipulation of a single actin filament by glass needles," *Nature*, Vol. 334, pp. 74-76, 1988.
- [10] A. Ishijima, H. Kojima, H. Higuchi, Y. Harada, T. Funatsu, and T. Yanagida, "Multiple and single-molecule analysis of the actomyosin motor by nanometer piconewton manipulation with a microneedle: unitary steps and forces," *Biophysical J.*, Vol. 70, pp. 383-400, 1996.
- [11] M. Tokunaga, T. Aoki, M. Hiroshima, K. Kitamura, and T. Yanagida, "Subpiconewton intermolecular force microscopy," *Biochem. Biophys. Res. Commun.*, Vol. 231, pp. 566-569, 1997.
- [12] U. Dammer, O. Popescu, P. Wagner, D. Anselmetti, H.J. Guntherodt, and G.N. Misevic, "Binding strength between cell adhesion proteoglycans measured by atomic force microscopy," *Science*, Vol. 267, pp. 1173-1175, 1995.
- [13] A.F. Oberhauser, P.E. Marszalek, H.P. Erickson, and J.M. Fernandez, "The molecular elasticity of the extracellular matrix protein tenascin," *Nature*, Vol. 393, pp. 181-185, 1998.
- [14] G.T. Charras, P.P. Lehenkari, and M.A. Horton, "Atomic force microscopy can be used to mechanically stimulate osteoblasts and evaluate cellular strain distribution," *Ultramicroscopy*, Vol. 86, pp. 85-95, 2001.
- [15] F.J. Alenghat, B. Fabry, K.Y. Tsai, W.H. Goldmann, and D.E. Ingber, "Analysis of cell mechanics in single vinculin-deficient cells using a magnetic tweezer," *Biochem. Res. Commun.*, Vol. 277, pp. 93-99, 2000.
- [16] V. Heinrich and R.E. Waugh, "A piconewton force transducer and its application to measurement of the bending stiffness of phospholipid membranes," *Ann. Biomed. Eng.*, Vol. 24, pp. 595-605, 1996.
- [17] J.N. Fass and D.J. Odde, "Tensile force dependent neurite elicitation via anti- $\beta 1$ integrin antibody-coated magnetic beads," *Biophysical J.*, Vol. 85, pp. 623-636, 2003.
- [18] E. Evans, "Looking inside molecular bonds at biological interfaces with dynamic force spectroscopy," *Biophys. Chem.*, Vol. 82, pp. 83-97, 1999.
- [19] R.M. Hochmuth, "Micropipette aspiration of living cells," *J. of Biomechanics*, Vol. 33, pp. 15-22, 2000.
- [20] C. Tomasi and T. Kanade, "Shape and motion from image streams: a factorization method," Technical Report CMU-CS-91-172, Carnegie Mellon University, Pittsburgh, PA, 1991.
- [21] R.M. Voyles, J.D. Morrow, and P.K. Khosla, "The shape from motion approach to rapid and precise force/torque sensor calibration," *J. of Dynamic Systems, Measurement and Control*, Vol. 119, No. 2, pp. 229-235, 1997.
- [22] D. Piyabongkarn, Y. Sun, R. Rajamani, A. Sezen, and B.J. Nelson, "Travel range extension of MEMS electrostatic microactuators," *IEEE Trans. on Control Systems Technology*, Vol. 13, No. 1, pp. 138-145, 2005.